

Towards Open-Ended Visual Scientific Discovery with Sparse Autoencoders

Samuel Stevens*, Jacob Beattie, Tanya Berger-Wolf and Yu Su
 The Ohio State University

Abstract

Scientific archives now contain hundreds of petabytes of data across genomics, ecology, climate, and molecular biology that could reveal undiscovered patterns if systematically analyzed at scale. Large-scale, weakly-supervised datasets in language and vision have driven the development of foundation models whose internal representations encode structure (patterns, co-occurrences and statistical regularities) beyond their training objectives. Most existing methods extract structure only for pre-specified targets; they excel at confirmation but do not support open-ended discovery of unknown patterns. We ask whether sparse autoencoders (SAEs) can enable open-ended feature discovery from foundation model representations. We evaluate this question in controlled rediscovery studies, where the learned SAE features are tested for alignment with semantic concepts on a standard segmentation benchmark and compared against strong label-free alternatives on concept-alignment metrics. Applied to ecological imagery, the same procedure surfaces fine-grained anatomical structure without access to segmentation or part labels, providing a scientific case study with ground-truth validation. While our experiments focus on vision with an ecology case study, the method is domain-agnostic and applicable to models in other sciences (e.g., proteins, genomics, weather). Our results indicate that sparse decomposition provides a practical instrument for exploring what scientific foundation models have learned, an important prerequisite for moving from confirmation to genuine discovery.

1. Introduction

Scientific data now spans hundreds of petabytes across domains, far outpacing what any lab can annotate or manually inspect.¹ Large neural networks trained on these datasets cover proteins (e.g., AlphaFold 3 [1]), weather (e.g., Graph-Cast, GenCast [34, 47]), genomics (e.g., scGPT, ESM3

*Corresponding author: stevens.994@osu.edu

¹For example, the NIH Sequence Read Archive exposes roughly 47 PB of public sequencing data, the European Nucleotide Archive provides roughly 63 PB of immediately downloadable data, NASA Earthdata (EOSDIS) hosts more than 120 PB of open Earth science data, and a single reanalysis, ERA5, is on the order of 5 PB.

[12, 23]), and vision (e.g., Scale-MAE, BioCLIP 2 [19, 48]). These models achieve strong predictive performance across a variety of tasks by learning compressed representations of the underlying data distribution's structure.

However, current usage of such foundation models in science is predominantly task-centric: models are used as frozen feature extractors or fine-tuned for specific predictions (species classification [57], cellular responses to perturbations [49], 3-D protein structure [21, 46]). The learned, compressed representations are high-dimensional embeddings optimized for task performance. While these representations enable accurate predictions, they do not directly provide reusable scientific measurements or expose the structure the model learned for systematic investigation. This limits foundation models to *confirmatory* applications where the target concepts are pre-specified (see Tab. 1).

Discovery vs. Confirmation Scientific discovery often involves establishing names and descriptions of previously unexplained phenomena in the world [33]. A morphological feature that distinguishes subspecies but is not formally cataloged, an unexplored correlation between climate variables, or a sequence motif in an understudied protein family: these cannot be found by methods that require specifying target concepts in advance.

Foundation models trained on millions of samples have processed more data than any human could learn from. If these models have learned semantic patterns not captured by existing annotations, interpretability methods offer a route to systematically surface this learned structure. However, current interpretability approaches require specifying concepts:

- Supervised probing tests for known concepts [4].
- Concept activation vectors (CAV) measure sensitivity to user-defined concepts [31].
- Saliency maps and attention visualizations explain individual predictions for predefined tasks [50, 53, 55].

These methods excel at *confirmation*, but cannot perform open-ended exploration to generate hypotheses about what patterns exist in the learned representations. When labels are scarce and salient factors are unknown (i.e., in scientific use cases), the inability to extract unnamed patterns from foundation models represents a significant limitation. If foundation models have learned meaningful patterns from data that ex-

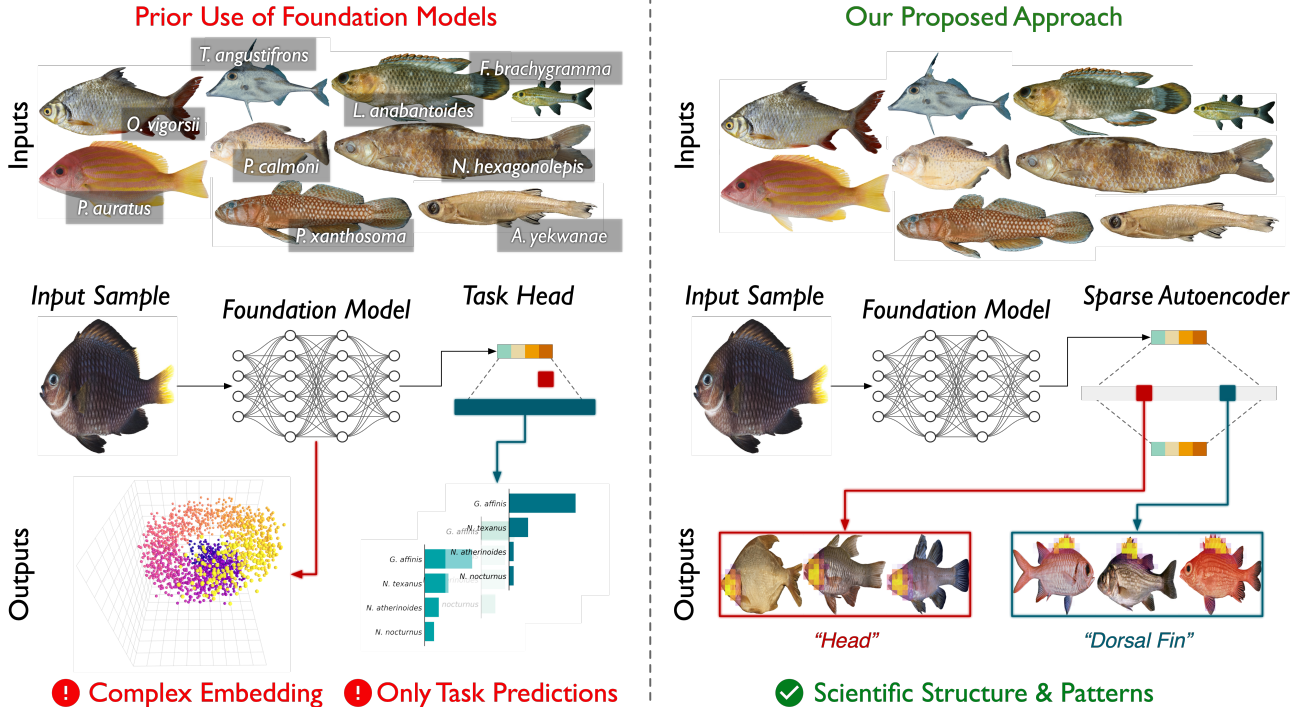


Figure 1. *Validating an instrument for open-ended feature discovery.* **Left:** Typical use of a foundation model in science: an input image is passed through a pretrained encoder and a task-specific head to yield class scores; the dense representation remains an opaque embedding, so unnamed factors are inaccessible. **Right:** Our procedure composes a foundation model with a sparse autoencoder, producing a library of interpretable semantic concepts with per-example activation maps. We find that these concepts align with and localize anatomical parts (e.g., head, dorsal fin) without seeing part-of-body labels. Fish images are shown as a case study with known anatomy providing a controlled rediscovery test; the explored method is domain-agnostic.

ceed what humans can manually analyze, we need methods to surface those patterns without pre-specification [27]. We view such open-ended feature discovery as a prerequisite step toward scientific discovery.

Our approach. To address this gap, we study sparse autoencoders (SAEs) as a candidate mechanism for decomposing foundation model representations into interpretable features without concept supervision [7, 13, 17, 56]. SAEs learn an overcomplete dictionary that reconstructs model activations through sparse linear combinations, with sparsity encouraging individual features to capture coherent semantic units. Unlike supervised methods, SAEs require no concept labels during training. Each learned feature provides a per-example activation score together with its decoding direction and exemplar evidence, enabling systematic investigation of what patterns the model represents. In short, we treat SAEs as a candidate tool for open-ended feature discovery from foundation models and seek to rigorously evaluate that tool in controlled settings [45].

Evidence. We train SAEs on patch-level activations from DINOv3 [52], a self-supervised vision transformer (ViT, [15]). We evaluate if SAEs can recover fine-grained seman-

tic structure without access to labels in two settings: (1) ADE20K scene segmentation [63], containing 150 object classes, and (2) ecological images, where we test recovery of anatomical body parts from the FishVista dataset [39, 40]. Both settings provide known semantic structure, so they serve as controlled rediscovery tests of whether SAEs can recover concepts that domain experts already recognize. We find that SAEs reliably extract semantic concepts that were never explicitly labeled in DINOv3’s self-supervised training objective. We compare against decomposition baselines (k -means clustering and PCA) and find that SAEs achieve substantially higher concept alignment, with Matryoshka SAEs [8] reaching 7.9% higher class coverage than standard SAEs on ADE20K (see Sec. 4.1 and Tab. 2 for details).

Our results indicate that unsupervised sparse decomposition can systematically recover semantic structure from foundation model representations. On standard vision benchmarks, SAEs rediscover segmentation classes and spatial relationships without label access during training. On scientific images, they surface fine-grained anatomical features, providing measurable quantities that can be evaluated against biological annotations. We analyze when this approach succeeds and when it fails, documenting sensitivity to archi-

Table 1. Comparison of methods for extracting knowledge from foundation models. Most approaches require researchers to specify concepts or tasks in advance, limiting them to confirmatory analysis. SAEs support open-ended feature discovery by surfacing the model’s learned feature vocabulary in a structured format without any supervision.

Method	Input	Output	Example	Discovery?
Task Heads	Labeled task dataset	Task predictions	Species classification	✗ Needs task labels
Linear Probes	Labeled concept \mathcal{A} samples	Decodability of concept \mathcal{A}	“Does DINOv3 see eyes?”	✗ Pre-specified concepts
Concept Vec.	Labeled concept \mathcal{A} samples	Score for concept \mathcal{A}	“Find a ‘striped’ direction”	✗ Needs concept samples
Feature Viz.	Selected neuron	Synthetic images	“DeepDream for neuron j ”	✗ Unstructured output
Prototypes	Labeled task dataset	Task-tied prototypes	“This looks like concept \mathcal{B} ”	✗ Task-specific
SAEs (Ours)	Unlabeled activations	Interpretable features	Discover new traits	✓ Finds unknown patterns

tectural choices, layer selection, and dataset characteristics. While we validate our approach on two vision domains, the protocol itself is domain-agnostic and applicable to any setting with foundation model representations: proteins, genomics, weather, and more [1, 12, 34]. We view this work as a prerequisite step: establishing that SAEs can systematically recover known structure before using them to search for truly novel scientific phenomena.

2. Related Work

Foundation Models. Domain-specific foundation models capture rich structure and achieve state-of-the-art performance on their focal tasks, as shown in proteins [1, 23], ecology [54], weather [34, 47], and single-cell genomics [12]. In both general and scientific domains, large-scale training leads to emergent abilities beyond the pre-training objective [19, 60]. Theory and evidence suggest that large pretrained models internalize meaningful structure [9, 20, 28, 36]. Despite this, most scientific models are benchmarked as **task-specific predictors** rather than sources of novel concepts.

Interpretability Methods. A large body of work explains predictions without exposing a global factorization of representations. Saliency and attribution methods (e.g., gradients, Integrated Gradients, Grad-CAM) highlight input regions for *individual* decisions and have known validity pitfalls [2, 50, 53, 55]. Linear probes test separability of *pre-specified* targets [4, 25]; concept methods such as TCAV/ACE require exemplar sets and so test investigator-defined ideas [18, 31]. Prototype models (ProtoPNet, ProtoTree, ProtoPFormer) provide case-based, class-tied explanations but are trained end-to-end for specific tasks [11, 41, 61]. Activation maximization and “feature visualization” (DeepDream-style) optimize inputs for chosen units to aid intuition, but produce synthetic, non-natural images [38, 42, 43]. These approaches excel at explaining predictions or testing for known concepts (confirmation) but cannot be used to discover patterns without prior specification.

Sparse Autoencoders & Decomposition. Classical dictionary learning and sparse coding demonstrated that sparse, parts-based factors can emerge from natural data [3, 37, 44]. Recent work applies sparse autoencoders (SAEs) to model activations, showing that sparse decompositions can partially “unmix” superposed features and yield monosemantic directions [7, 16, 17] in language and vision models. SAEs address the superposition hypothesis [16] by assigning features to directions in activation space rather than individual neurons. Gao et al. demonstrate that k -sparse autoencoders scale effectively and improve reconstruction-sparsity trade-offs. Concurrent work argues for using SAEs for discovering unknown concepts rather than acting on known ones [45] and applies dictionary learning to microscopy foundation models for biological concept extraction [14].

Discovery. We use *discovery* to mean surfacing previously unnamed factors (morphological features distinguishing subspecies, correlations between climate variables, or conserved sequence motifs in understudied proteins) as opposed to *confirmation* of pre-specified targets. Closest in intent to our goal are (i) work advocating SAEs for uncovering *unknown* concepts rather than acting on *known* ones [45] and (ii) dictionary-learning approaches that extract biological concepts from microscopy foundation models [14]. We differ by targeting dense token representations in vision and validating both on a standard semantic benchmark and an ecology case study. We also differ from unsupervised dense segmentation methods (LOST, TokenCut, STEGO, MaskCut) by returning global features with per-patch activations rather than per-image masks or clusters [22, 51, 58, 59].

Methods for open-ended, unsupervised discovery from foundation model representations remain underdeveloped. Our work takes a step toward addressing this gap by demonstrating, in controlled rediscovery settings, that sparse decomposition of foundation model representations can systematically surface semantic structure.

3. Methodology

We ask the question: “Can SAEs reliably rediscover unlabeled concepts in pre-trained models?” Because discovery demands finding unnamed structure rather than confirming known categories, our method avoids concept supervision and treats labels only as holdout probes. Our goal is to recover a dictionary whose latents serve as candidate concepts and other interpretable features that can be measured and compared across images. We outline the ViT feature extraction, the SAE objective, and the evaluation probes that operationalize this goal.

Foundation Model. We use the publicly available DINOv3 ViT-L/16 checkpoint [52]. Images are resized to 256×256 with bicubic interpolation, yielding a 16×16 grid of patches per image. We extract patch-token activations ([CLS] discarded) from the final (24th) layer.

Sparse Autoencoders (SAEs). Our dictionary learner is a ReLU SAE [7, 56]; given a d -dimensional activation vector $\mathbf{x} \in \mathbb{R}^d$ from an intermediate layer l of a transformer, an SAE maps \mathbf{x} to a sparse representation $f(\mathbf{x})$ (Eqs. (1) and (2)) and reconstructs the original input (Eq. (3)):

$$\mathbf{h} = W_{\text{enc}}(\mathbf{x} - b_{\text{dec}}) + b_{\text{enc}} \quad (1)$$

$$f(\mathbf{x}) = \text{ReLU}(\mathbf{h}) \quad (2)$$

$$\hat{\mathbf{x}} = W_{\text{dec}} f(\mathbf{x}) + b_{\text{dec}} \quad (3)$$

where $W_{\text{enc}} \in \mathbb{R}^{n \times d}$, $b_{\text{enc}} \in \mathbb{R}^n$, $W_{\text{dec}} \in \mathbb{R}^{d \times n}$ and $b_{\text{dec}} \in \mathbb{R}^d$. The training objective minimizes reconstruction error while encouraging sparsity:

$$\mathcal{L}(\theta) = \|\mathbf{x} - \hat{\mathbf{x}}\|_2^2 + \lambda \mathcal{S}(f(\mathbf{x})) \quad (4)$$

where λ controls the sparsity penalty and \mathcal{S} measures sparsity (L_1 norm for training, L_0 for model selection).

We train 16,384-latent SAEs for 100M patches and sweep a logarithmic grid of sparsity coefficients λ and learning rates. We summarize each trained model by its reconstruction quality (normalized MSE) and sparsity (L_0). Normalized MSE (NMSE) is MSE normalized by a mean baseline MSE:

$$\text{NMSE} = \frac{\sum_i \|\mathbf{x}_i - \hat{\mathbf{x}}_i\|_2^2}{\sum_i \|\mathbf{x}_i - \bar{\mathbf{x}}\|_2^2} \quad (5)$$

where $\hat{\mathbf{x}}_i$ is the predicted reconstruction and $\bar{\mathbf{x}}$ is the mean of all \mathbf{x}_i .

Matryoshka SAEs. To avoid feature splitting [7, 10, 35], we use Matryoshka SAEs [8], which learn a single SAE by training multiple nested dictionaries simultaneously. Each training step samples random prefixes of SAE latents and reconstructs the inputs using each sampled prefix. We sample ten prefixes $\mathcal{M} = m_1, m_2, \dots, m_{10} \subset [1, 16384]$, meaning the first m_1 latents are used to reconstruct the input, then

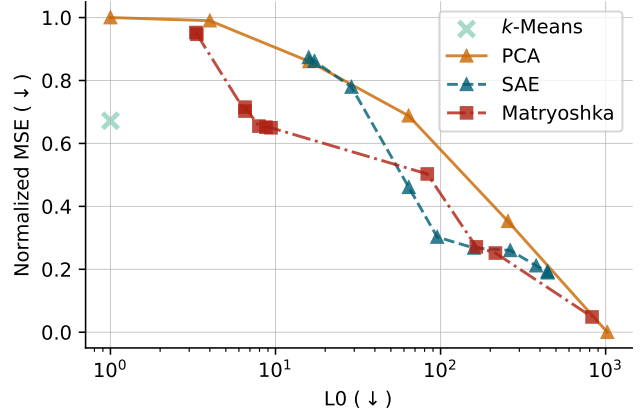


Figure 2. We compare k -means, PCA, vanilla SAEs and Matryoshka SAEs along the reconstruction-sparsity tradeoff for learning to decompose ViT patch activations. We use final layer activations from DINOv3 ViT-L/16 on ImageNet-1K; we fit all methods on the training split and measure normalized MSE (see Eq. (5)) and L_0 on the validation split. For k -means, we “reconstruct” every patch with its nearest centroid; thus, L_0 is always 1. For PCA, we sweep the number of components. For both SAE variants, we sweep λ and show the Pareto frontier of reconstruction-sparsity. **Takeaway:** Reconstruction-sparsity does not indicate an optimal method.

the first m_2 latents, etc. The sum of MSE values from each prefix reconstruction is then used in place of MSE in the objective function:

$$\mathcal{L}(\theta) = \sum_{m \in \mathcal{M}} \|\mathbf{x} - \hat{\mathbf{x}}_{0:m}\|_2^2 + \lambda \mathcal{S}(f(\mathbf{x})) \quad (6)$$

where $\hat{\mathbf{x}}_{0:m}$ is the reconstruction using only the first m latents. This training regime forces early latents to capture more general features. Following training, Matryoshka SAE inference is identical to vanilla SAEs, and their reconstruction quality can be evaluated using normalized MSE.

4. Experiments

We evaluate whether sparse autoencoders can systematically recover semantic structure from foundation model representations without concept supervision via **controlled rediscovery**: we train SAEs on unlabeled data, then test whether the learned features align with ground-truth semantic concepts that were withheld during training. Strong alignment on known concepts validates the method and provides a foundation for applying it to domains where ground truth is unavailable or incomplete. We organize our experiments around three questions. **Q1:** Do SAE features align with known segmentation concepts on a standard benchmark? **Q2:** Do the same procedures surface anatomical parts in an ecological case study? **Q3:** How does foundation model size and depth affect downstream concept alignment?

(a) *k*-means

(b) PCA

(c) Vanilla SAE

(d) Matryoshka SAE

Figure 3. Top images for lowest-loss probes for “person” (left) and “toilet” (right) classes for each method. **(a):** *k*-means does not recover the “person” class; the best “person” cluster fires on roads. **(b):** PCA learns a “person” component, but does not consistently activate on the entire person. Furthermore, PCA does not recover the “toilet” class; the best “toilet” doesn’t have an obvious semantic concept. **(c) & (d):** Vanilla and Matryoshka SAEs both reliably recover both “person” and “toilet” and activate on the entire object. **Takeaway:** While *k*-means and PCA are good by dictionary learning metrics, visual concepts recovered by both vanilla and Matryoshka SAEs are more consistent and salient.

We evaluate concept alignment on held-out activations from ADE20K for rediscovery and from FishVista for the ecology case study. We compare against label-free alternatives (*k*-means and PCA) and report the reconstruction-sparsity trade-off (normalized MSE vs. L_0). We measure concept alignment by fitting binary logistic regression classifiers (ridge-regularized, per-class) on SAE activations, following prior work in SAEs for language models [17]. For each concept, we train a 1-D logistic on each SAE latent i ’s activations z_i and record the best loss across all latents for each class:

$$\min_{i,w,b} \mathbb{E}[-y \log \sigma(wz_i+b) - (1-y) \log(1-\sigma(wz_i+b))] \quad (7)$$

We report (1) probe R : loss \mathcal{L} normalized by a bias-only loss \mathcal{L}_π : $1 - (\mathcal{L}/\mathcal{L}_\pi)$, (2) mean Average Precision (mAP) across all classes, (3) Purity@ k : precision of the top- k activated patches for each feature, and (4) Coverage@ τ : the fraction of classes whose best-aligned feature achieves AP $\geq \tau$. For each class, we select the single SAE feature with lowest binary cross-entropy on the training set, enabling unsupervised feature-to-concept matching. We report downstream ADE20K validation metrics for the SAE with the best probe loss on the ADE20K training split. This protocol tests whether SAEs produce features that align with semantic concepts.

Table 2. SAEs for rediscovering ADE20K’s semantic segmentation classes from DINOv3 ViT-L/16. For each method, we choose the best layer from DINOv3 based on probe loss (Eq. (7) on ADE20K’s training split and report ADE20K validation metrics. Probe R is normalized probe loss, as described in Sec. 4. Purity@ k is precision over the top- k highest-scoring patches for a feature, where $k = 16$. Coverage@ τ is the fraction of ADE20K classes with best AP $\geq \tau$, where $\tau = 0.3$. **Takeaway:** Matryoshka SAEs demonstrate meaningful improvement over traditional unsupervised methods and vanilla SAEs on downstream metrics.

Method	Dict. \downarrow		Downstream \uparrow			
	NMSE	L_0	Probe R	mAP	Purity@ k	Cov@ τ
<i>k</i> -Means	0.619	1	0.001	0.031	0.795	0.026
PCA	0.352	256	0.259	0.093	0.612	0.079
SAE	0.460	64.1	0.425	0.313	0.748	0.417
Matryoshka	0.702	6.5	0.402	0.319	0.808	0.450

4.1. Rediscovering Semantic Segmentations

We use ADE20K (150 classes) as a standard testbed for controlled rediscovery: can label-free SAE features align with segmentation classes? SAEs are trained on ImageNet-1K activations only; ADE20K labels enter solely at evaluation, isolating extraction from supervision. Concretely, we extract activations on ImageNet-1K (train/val) and ADE20K

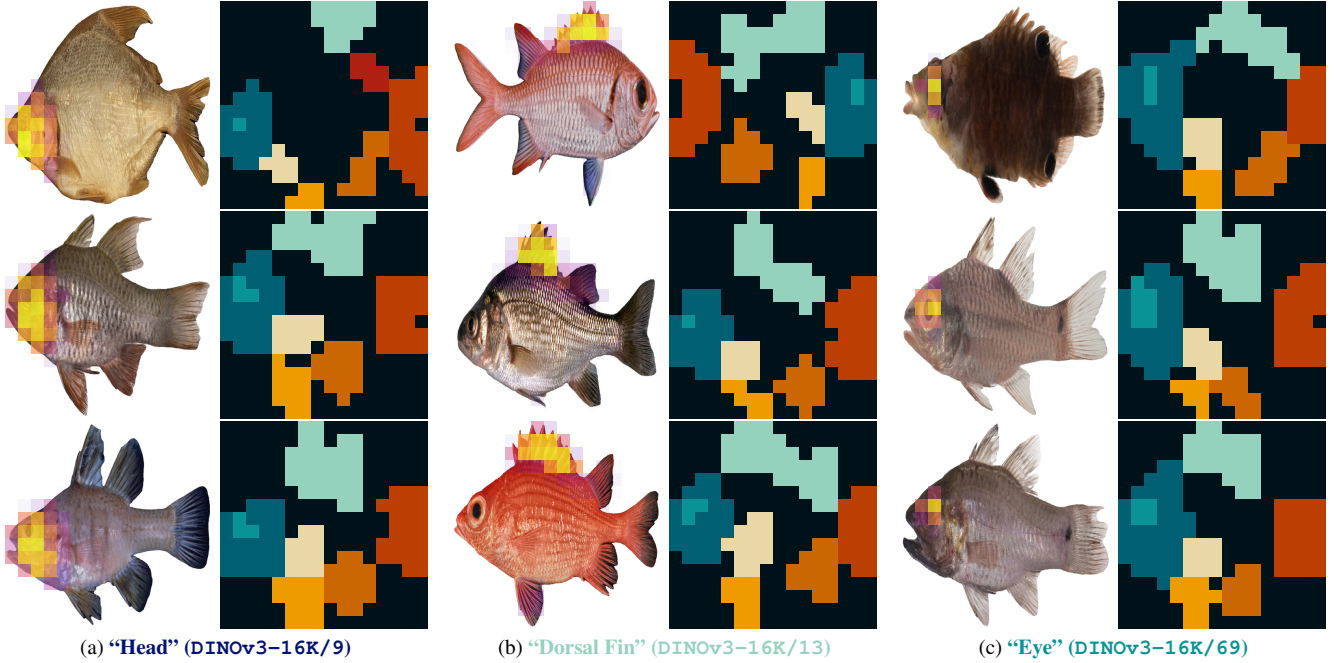


Figure 4. Example Matryoshka SAE features (left) and patch-level segmentation masks (right) for (a) “Head”, (b) “Dorsal Fin” and (c) “Eye” from DINOv3 ViT-L/16. Features were picked by minimizing cross entropy on binary classification for each body part, as described in Sec. 4.2 and Eq. (7). **Takeaway:** Matryoshka SAEs accurately learn scientific concepts (anatomical body parts) without labels.

(train/val) from the final layer of DINOv3 ViT-L/16.

Baseline Methods. We compare SAEs to two standard unsupervised machine learning methods: k -means and principal component analysis (PCA). We fit k -means and PCA on ImageNet-1K training activations. For k -means, we use $k=16,384$ clusters and use the nearest cluster as the predicted reconstruction with a fixed $L_0=1$. We fit PCA with n components $n \in \{1, 4, 16, 64, 256, 1024\}$. We report normalized reconstruction MSE on ImageNet-1K (validation split).

Results. We compare all methods on the reconstruction-sparsity tradeoff in Fig. 2, report rediscovery metrics in Tab. 2 and show qualitative examples in Fig. 3. While both SAE variants do not improve upon classical baselines as measured by normalized MSE and sparsity, they *do* lead to better concept discovery as measured by mAP, Purity@ k and Coverage@ τ . Matryoshka SAEs, similar to PCA, also implicitly order their latents in order of decreasing reconstruction importance. Anecdotally, this makes it easier to browse for salient, “interesting” concepts.

Discussion. k -means and PCA are competitive on reconstruction-sparsity trade-offs, yet underperform SAEs on downstream concept-alignment metrics such as mAP, Purity@ k , and Coverage@ τ . This reinforces that normalized MSE and L_0 measure how well activations are compressed, not how well individual latents track semantic concepts. Prior work in evaluating SAEs for language model

Table 3. Matryoshka SAEs for concept rediscovery on general domain (ADE20K) and an ecological case study (FishVista). FishVista images are a more homogeneous distribution compared to ADE20K; we hypothesize that this contributes to the improved reconstruction (NMSE).

Dataset	Dict. ↓		Downstream ↑			
	NMSE	L_0	Probe R	mAP	Purity@ k	Cov@ τ
ADE20K	0.702	6.5	0.402	0.319	0.808	0.45
FishVista	0.150	75.1	0.440	0.610	0.931	0.90

interpretability also finds dictionary-learning metrics insufficient [30].

4.2. Can SAEs recover domain-specific concepts?

Beyond the general-domain semantic concepts present in ADE20K, we ultimately want SAEs to support scientific discovery. In this work, we again evaluate that capability via rediscovery: can vision foundation models, in combination with SAEs, rediscover the anatomy of diverse fish species? We use FishVista [39, 40] and the 10 annotated body-part traits to answer this question (see Fig. 4 for dataset examples). We train SAEs on 56.3K fish images and evaluate SAE discovery on the 4.6K (disjoint) images with body part segmentations.

Results. We find that Matryoshka SAEs reliably find domain-specific concepts; we compare results on ADE20K

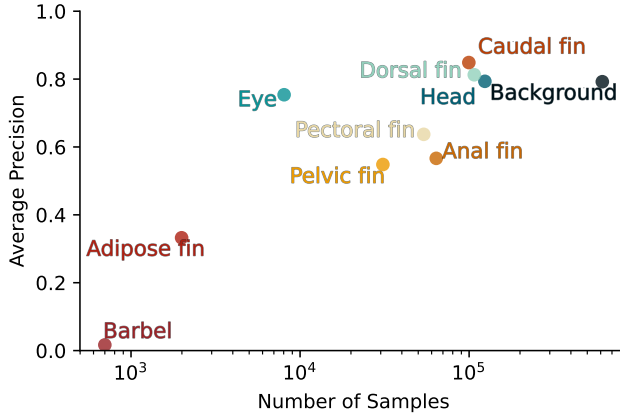


Figure 5. Prevalence vs rediscovery on FishVista. Each point is a body part; x-axis: number of patch-level samples in the validation split, y-axis: AP of the best-matching (lowest probe loss) Matryoshka SAE latent. More common body parts are rediscovered more reliably. **Takeaway:** Higher concept prevalence improves label-free rediscovery.

and FishVista in Tab. 3, show examples in Fig. 4 and compare concept prevalence with average precision in Fig. 5. These results indicate that strong foundation models, in combination with SAEs, can surface features that align closely with expert-defined anatomical annotations. Furthermore, the Matryoshka objective naturally orders latents from most to least general; we (anecdotally, but consistently) found earlier latents more “interesting” than later latents.

Discussion. Body parts that occur in more patches are recovered with higher average precision (Fig. 5), while rare parts are substantially harder to rediscover. This implies that scientific applications targeting rare or long-tail structures and patterns may need either more data, targeted sampling, or novel dictionary learning algorithms that learn rare structures more efficiently.

4.3. Do larger models improve concept rediscovery?

Model scale consistently correlates with downstream performance [26, 29]. Prior work proposes scaling laws for SAE reconstruction based on both SAE and foundation model size [17] but does not investigate downstream performance. We assess foundation model size effects by training SAEs on patch activations from DINOv3 ViT-S/16, ViT-B/16, and ViT-L/16 checkpoints. The models vary in both total parameter count (22M, 86M and 303M, respectively) and the embedding dimension d (384, 768, and 1,024, respectively). For each size, we keep the SAE width fixed at 16,384, train on ImageNet-1K 100M patch activations and probe the SAEs for ADE20K features.

Results. In Fig. 6 we see that larger models are in fact harder to reconstruct (note that the y-axis is *raw* rather than

Table 4. SAEs on different sizes of DINOv3 for rediscovering ADE20K’s semantic segmentation classes. **Takeaway:** While larger ViTs are harder to reconstruct, they lead to better concept rediscovery.

ViT	Dict. \downarrow		Downstream \uparrow			
	NMSE	L_0	Probe R	mAP	Purity@ k	Cov@ τ
ViT-S/16	0.293	95.0	0.433	0.203	0.742	0.245
ViT-B/16	0.359	89.8	0.440	0.312	0.811	0.430
ViT-L/16	0.702	6.5	0.402	0.319	0.808	0.450

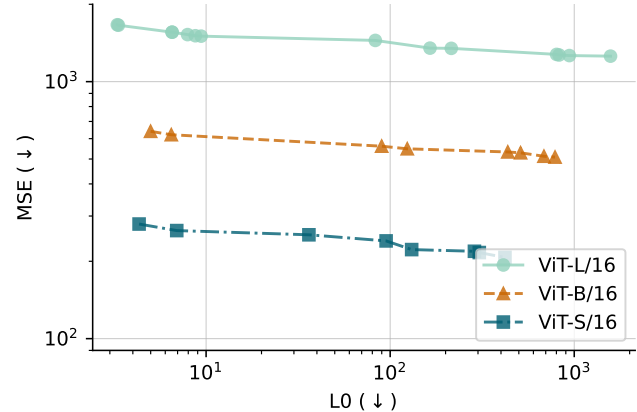


Figure 6. The reconstruction–sparsity tradeoff for SAEs trained on different sized ViTs. Larger backbones are harder to reconstruct at a given sparsity (ViT-L/16 > ViT-B/16 > ViT-S/16), though all improve as L_0 increases. Note that the y-axis is *raw* rather than normalized MSE.

normalized MSE), consistent with prior work in scaling SAEs for language models [17]. Despite more challenging dictionary learning, we see in Tab. 4 that SAEs applied to larger models both recover more concepts (coverage) and are more precise (purity). All three sizes of the DINOv3 ViTs are distilled from a single, larger teacher model [52]; we conjecture then that all three checkpoints have learned the same set of concepts. These results indicate that, at least for vision, strong foundation models in combination with SAEs can rediscover semantic concepts, which we view as a prerequisite for scientific discovery.

Discussion. A potential confounder is total training FLOPs: prior work shows that additional SAE training compute (total FLOPs) leads to stronger SAEs as measured by the reconstruction–sparsity tradeoff [17]. Our SAEs trained on larger embedding dimensions d use more compute during training; this could explain the stronger results for larger models. However, our SAEs trained on larger models have *worse* reconstruction–sparsity but *better* downstream concept alignment metrics.

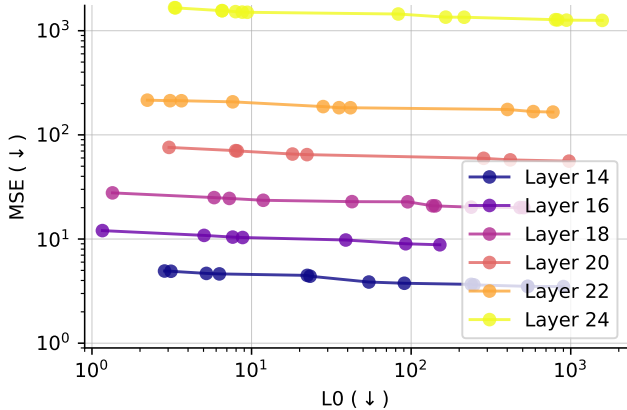


Figure 7. Layer-wise reconstruction-sparsity trade-off (DINOv3 ViT-L/16) on ImageNet-1K activations. Each curve is a ViT layer (14–24). Later layers consistently incur higher MSE at matched sparsity, indicating greater representational complexity. Again, note that the y -axis is *raw* rather than normalized MSE.

4.4. Which layer is best?

Representations evolve across network depth: later layers in CNNs and ViTs tend to encode higher-level, more linearly separable semantics, which often improves transfer and dense alignment [5, 9, 62]. However, recent results show that the final layer is not always optimal [6]. Intermediate layers can yield less entangled, more spatially localized features depending on the downstream task. We therefore evaluate six layers in the second half of the transformer for the three evaluated checkpoints: for the 24-layer ViT-L/16 model, we use layers 14, 16, 18, 20, 22, and 24 and for the 12-layer ViT-S/16 and ViT-B/16 we use the last 6 layers 7, 8, 9, 10, 11, and 12.

Results. In Fig. 7, we find that later layers are harder to reconstruct (note that the y -axis is *raw* rather than normalized MSE). We also evaluate downstream metrics (mAP) for the best SAE at each layer for all three ViT checkpoints in Fig. 8. Despite more challenging reconstruction, we find that later layers lead to better recovery for all three checkpoints.

Discussion. Prior work in SAEs for language models finds that later layers are harder to reconstruct except for the final two layers [17]. Language models use a linear embedding layer for next-token-prediction; the final layers must optimize for linear separability. In contrast, DINOv3 uses multiple, loss-specific multilayer perceptrons with additional non-linearities for pre-training [52]; we conjecture this architectural difference leads to the difference in our results.

5. Conclusion

In the settings we studied, we demonstrated that sparse autoencoders can systematically recover semantic structure

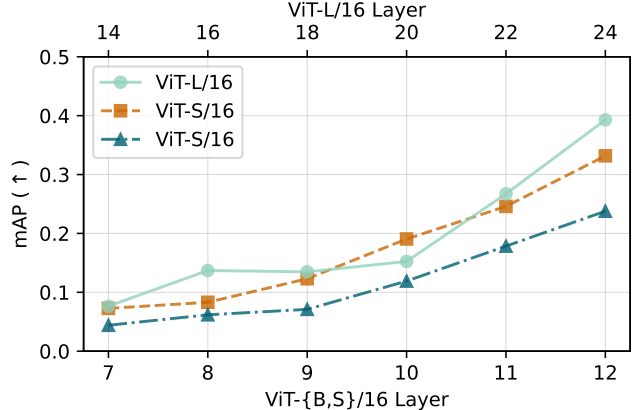


Figure 8. Matryoshka SAE probe quality as measured by mean average precision (mAP) for DINOv3 ViT-S/16, ViT-B/16 and ViT-L/16 checkpoints over different transformer layers. **Takeaway:** Despite larger ViTs and later layers being harder to reconstruct at a given sparsity (see Figs. 6 and 7), larger ViTs and later layers lead to better SAE concept alignment.

from foundation model representations without concept supervision, using controlled rediscovery on both general-domain visual concepts and a scientific case study. On ADE20K, SAEs consistently rediscovered semantic units from DINOv3 activations trained only on ImageNet-1K, outperforming decomposition baselines (k -means & PCA) on concept alignment metrics. On ecological images, the same procedure surfaced anatomical structures without using segmentation or part labels during extraction. Our results provide evidence that SAEs are a practical method for extracting interpretable features from vision foundation models, complementing existing confirmatory approaches. SAEs’ exploratory capabilities are well-suited to scientific domains where target concepts are not fully specified in advance. Importantly, our contributions should be understood as validating SAEs as an instrument for open-ended feature discovery, not as delivering novel biological or physical discoveries themselves.

As domain-specific foundation models proliferate across scientific fields, methods for understanding what these models learned become increasingly important. Our results indicate that sparse decomposition provides a practical route from high-dimensional representations to interpretable visual features. Rather than treating foundation models solely as feature extractors for predefined tasks, SAE-based decomposition enables researchers to investigate what patterns models captured from data, generate hypotheses about unexpected structures, and establish reproducible measurements across studies. While our validation focuses on vision with ecology as a case study, the approach applies wherever foundation models learn from unlabeled or weakly-labeled data at scales that exceed manual analysis.

References

[1] Josh Abramson, Jonas Adler, Jack Dunger, Richard Evans, Tim Green, Alexander Pritzel, Olaf Ronneberger, Lindsay Willmore, Andrew J Ballard, Joshua Bambrick, et al. Accurate structure prediction of biomolecular interactions with alphafold 3. *Nature*, 630(8016):493–500, 2024. 1, 3

[2] Julius Adebayo, Justin Gilmer, Michael Muelly, Ian Goodfellow, Moritz Hardt, and Been Kim. Sanity checks for saliency maps. *Advances in neural information processing systems*, 31, 2018. 3

[3] Michal Aharon, Michael Elad, and Alfred Bruckstein. K-svd: An algorithm for designing overcomplete dictionaries for sparse representation. *IEEE Transactions on signal processing*, 54(11):4311–4322, 2006. 3

[4] Guillaume Alain and Yoshua Bengio. Understanding intermediate layers using linear classifier probes. *arXiv preprint arXiv:1610.01644*, 2016. 1, 3

[5] Hossein Azizpour, Ali Sharif Razavian, Josephine Sullivan, Atsuto Maki, and Stefan Carlsson. Factors of transferability for a generic convnet representation. *IEEE transactions on pattern analysis and machine intelligence*, 38(9):1790–1802, 2015. 8

[6] Daniel Bolya, Po-Yao Huang, Peize Sun, Jang Hyun Cho, Andrea Madotto, Chen Wei, Tengyu Ma, Jiale Zhi, Jathushan Rajasegaran, Hanoona Rasheed, et al. Perception encoder: The best visual embeddings are not at the output of the network. *arXiv preprint arXiv:2504.13181*, 2025. 8

[7] Trenton Bricken, Adly Templeton, Joshua Batson, Brian Chen, Adam Jermyn, Tom Conerly, Nick Turner, Cem Anil, Carson Denison, Amanda Askell, Robert Lasenby, Yifan Wu, Shauna Kravec, Nicholas Schiefer, Tim Maxwell, Nicholas Joseph, Zac Hatfield-Dodds, Alex Tamkin, Karina Nguyen, Brayden McLean, Josiah E Burke, Tristan Hume, Shan Carter, Tom Henighan, and Christopher Olah. Towards monosemanticity: Decomposing language models with dictionary learning. *Transformer Circuits Thread*, 2023. <https://transformer-circuits.pub/2023/monosemantic-features/index.html>. 2, 3, 4, 13

[8] Bart Bussmann, Noa Nabeshima, Adam Karvonen, and Neel Nanda. Learning multi-level features with matryoshka sparse autoencoders. *arXiv preprint arXiv:2503.17547*, 2025. 2, 4

[9] Mathilde Caron, Hugo Touvron, Ishan Misra, Hervé Jégou, Julien Mairal, Piotr Bojanowski, and Armand Joulin. Emerging properties in self-supervised vision transformers. In *Proceedings of the IEEE/CVF international conference on computer vision*, pages 9650–9660, 2021. 3, 8

[10] David Chanin, James Wilken-Smith, Tomáš Dulka, Hardik Bhatnagar, Satvik Golechha, and Joseph Bloom. A is for absorption: Studying feature splitting and absorption in sparse autoencoders. *arXiv preprint arXiv:2409.14507*, 2024. 4

[11] Chaofan Chen, Oscar Li, Daniel Tao, Alina Barnett, Cynthia Rudin, and Jonathan K Su. This looks like that: deep learning for interpretable image recognition. *Advances in neural information processing systems*, 32, 2019. 3

[12] Haotian Cui, Chloe Wang, Hassaan Maan, Kuan Pang, Fengning Luo, Nan Duan, and Bo Wang. scgpt: toward building a foundation model for single-cell multi-omics using generative ai. *Nature methods*, 21(8):1470–1480, 2024. 1, 3

[13] Hoagy Cunningham, Aidan Ewart, Logan Riggs, Robert Huben, and Lee Sharkey. Sparse autoencoders find highly interpretable features in language models. *arXiv preprint arXiv:2309.08600*, 2023. 2

[14] Konstantin Donhauser, Kristina Ulicna, Gemma Ellyse Moran, Aditya Ravuri, Kian Kenyon-Dean, Cian Eastwood, and Jason Hartford. Towards scientific discovery with dictionary learning: Extracting biological concepts from microscopy foundation models. *arXiv preprint arXiv:2412.16247*, 2024. 3

[15] Alexey Dosovitskiy. An image is worth 16x16 words: Transformers for image recognition at scale. *arXiv preprint arXiv:2010.11929*, 2020. 2

[16] Nelson Elhage, Tristan Hume, Catherine Olsson, Nicholas Schiefer, Tom Henighan, Shauna Kravec, Zac Hatfield-Dodds, Robert Lasenby, Dawn Drain, Carol Chen, Roger Grosse, Sam McCandlish, Jared Kaplan, Dario Amodei, Martin Wattenberg, and Christopher Olah. Toy models of superposition. *Transformer Circuits Thread*, 2022. https://transformer-circuits.pub/2022/toy_model/index.html. 3

[17] Leo Gao, Tom Dupre la Tour, Henk Tillman, Gabriel Goh, Rajan Troll, Alec Radford, Ilya Sutskever, Jan Leike, and Jeffrey Wu. Scaling and evaluating sparse autoencoders. In *The Thirteenth International Conference on Learning Representations*, 2025. URL <https://openreview.net/forum?id=tcsZt9ZNKD>. 2, 3, 5, 7, 8

[18] Amirata Ghorbani, James Wexler, James Y Zou, and Been Kim. Towards automatic concept-based explanations. *Advances in neural information processing systems*, 32, 2019. 3

[19] Jianyang Gu, Samuel Stevens, Elizabeth G Campolongo, Matthew J Thompson, Net Zhang, Jiaman Wu, Andrei Kopanov, Zheda Mai, Alexander E. White, James Balhoff, Wasila M Dahdul, Daniel Rubenstein, Hilmar Lapp, Tanya Berger-Wolf, Wei-Lun Chao, and Yu Su. BioCLIP 2: Emergent properties from scaling hierarchical contrastive learning. 2025. URL <https://bioclip2.org>

<https://arxiv.org/abs/2505.23883>. 1, 3

[20] David Ha and Jürgen Schmidhuber. World models. *arXiv preprint arXiv:1803.10122*, 2(3), 2018. 3

[21] Jürgen Haas, Alessandro Barbato, Dario Behringer, Gabriel Studer, Steven Roth, Martino Bertoni, Khaled Mostaguir, Rafal Gumienny, and Torsten Schwede. Continuous automated model evaluation (cameo) complementing the critical assessment of structure prediction in casp12. *Proteins: Structure, Function, and Bioinformatics*, 86:387–398, 2018. 1

[22] Mark Hamilton, Zhoutong Zhang, Bharath Hariharan, Noah Snavely, and William T. Freeman. Unsupervised semantic segmentation by distilling feature correspondences. In *International Conference on Learning Representations*, 2022. URL <https://openreview.net/forum?id=SaKO6z6H10c>. 3

[23] Thomas Hayes, Roshan Rao, Halil Akin, Nicholas J Sofroniew, Deniz Oktay, Zeming Lin, Robert Verkuil, Vincent Q Tran, Jonathan Deaton, Marius Wiggert, et al. Simulating 500 million years of evolution with a language model. *Science*, 387(6736):850–858, 2025. 1, 3

[24] Kaiming He, Xiangyu Zhang, Shaoqing Ren, and Jian Sun. Delving deep into rectifiers: Surpassing human-level performance on imagenet classification. In *Proceedings of the IEEE international conference on computer vision*, pages 1026–1034, 2015. 13

[25] John Hewitt and Percy Liang. Designing and interpreting probes with control tasks. In Kentaro Inui, Jing Jiang, Vincent Ng, and Xiaojun Wan, editors, *Proceedings of the 2019 Conference on Empirical Methods in Natural Language Processing and the 9th International Joint Conference on Natural Language Processing (EMNLP-IJCNLP)*, pages 2733–2743, Hong Kong, China, November 2019. Association for Computational Linguistics. doi: 10.18653/v1/D19-1275. URL https://aclanthology.org/D19-1275. 3

[26] Jordan Hoffmann, Sebastian Borgeaud, Arthur Mensch, Elena Buchatskaya, Trevor Cai, Eliza Rutherford, Diego de Las Casas, Lisa Anne Hendricks, Johannes Welbl, Aidan Clark, et al. Training compute-optimal large language models. *arXiv preprint arXiv:2203.15556*, 2022. 7

[27] Edward Hughes, Michael Dennis, Jack Parker-Holder, Feryal Behbahani, Aditi Mavalankar, Yuge Shi, Tom Schaul, and Tim Rocktaschel. Open-endedness is essential for artificial superhuman intelligence. *arXiv preprint arXiv:2406.04268*, 2024. 2

[28] Minyoung Huh, Brian Cheung, Tongzhou Wang, and Phillip Isola. Position: The platonic representation hypothesis. In *Forty-first International Conference on Machine Learning*, 2024. URL <https://openreview.net/forum?id=BH8TYy0r6u>. 3

[29] Jared Kaplan, Sam McCandlish, Tom Henighan, Tom B Brown, Benjamin Chess, Rewon Child, Scott Gray, Alec Radford, Jeffrey Wu, and Dario Amodei. Scaling laws for neural language models. *arXiv preprint arXiv:2001.08361*, 2020. 7

[30] Adam Karvonen, Can Rager, Johnny Lin, Curt Tigges, Joseph Isaac Bloom, David Chanin, Yeu-Tong Lau, Eoin Farrell, Callum Stuart McDougall, Kola Ayorinde, Demian Till, Matthew Wearden, Arthur Conmy, Samuel Marks, and Neel Nanda. SAE Bench: A comprehensive benchmark for sparse autoencoders in language model interpretability. In *Forty-second International Conference on Machine Learning*, 2025. URL <https://openreview.net/forum?id=qrU3yNfx0d>. 6

[31] Been Kim, Martin Wattenberg, Justin Gilmer, Carrie J Cai, James Wexler, Fernanda Viegas, and Rory Sayres. Interpretability beyond feature attribution: Quantitative testing with concept activation vectors (tcav). In *Proceedings of the 35th International Conference on Machine Learning*, 2018. 1, 3

[32] Diederik P Kingma and Jimmy Ba. Adam: A method for stochastic optimization. *arXiv preprint arXiv:1412.6980*, 2014. 13

[33] Thomas S Kuhn and Ian Hacking. *The structure of scientific revolutions*, volume 2. University of Chicago press Chicago, 1970. 1

[34] Remi Lam, Alvaro Sanchez-Gonzalez, Matthew Williamson, Peter Wirnsberger, Meire Fortunato, Ferran Alet, Suman Ravuri, Timo Ewalds, Zach Eaton-Rosen, Weihua Hu, et al. Learning skillful medium-range global weather forecasting. *Science*, 382(6677):1416–1421, 2023. 1, 3

[35] Patrick Leask, Bart Bussmann, Michael Pearce, Joseph Bloom, Curt Tigges, Noura Al Moubayed, Lee Sharkey, and Neel Nanda. Sparse autoencoders do not find canonical units of analysis. *arXiv preprint arXiv:2502.04878*, 2025. 4

[36] Yann LeCun. A path towards autonomous machine intelligence version 0.9. 2, 2022-06-27. *Open Review*, 62(1):1–62, 2022. 3

[37] Daniel D Lee and H Sebastian Seung. Learning the parts of objects by non-negative matrix factorization. *nature*, 401(6755):788–791, 1999. 3

[38] Aravindh Mahendran and Andrea Vedaldi. Visualizing deep convolutional neural networks using natural pre-images. *International Journal of Computer Vision*, 120(3):233–255, 2016. 3

[39] Kazi Saeed Mehrab, M. Maruf, Arka Daw, Harish Babu Manogaran, Abhilash Neog, Mridul Khrana, Bahadir Altintas, Yasin Bakis, Elizabeth G

Campolongo, Matthew J Thompson, Xiaojun Wang, Hilmar Lapp, Wei-Lun Chao, Paula M. Mabee, Henry L. Bart Jr. au2, Wasila Dahdul, and Anuj Karpatne. Fish-vista: A multi-purpose dataset for understanding & identification of traits from images, 2024. URL <https://arxiv.org/abs/2407.08027>. 2, 6

[40] Kazi Sajeed Mehrab, M. Maruf, Arka Daw, Harish Babu Manogaran, Abhilash Neog, Mridul Khurana, Bahadir Altintas, Yasin Bakış, Elizabeth G Campolongo, Matthew J Thompson, Xiaojun Wang, Hilmar Lapp, Wei-Lun Chao, Paula M. Mabee, Henry L. Bart Jr., Wasila Dahdul, and Anuj Karpatne. Fish-vista: A multi-purpose dataset for understanding & identification of traits from images, 2024. URL <https://huggingface.co/datasets/imageomics/fish-vista>. 2, 6

[41] Meike Nauta, Ron Van Bree, and Christin Seifert. Neural prototype trees for interpretable fine-grained image recognition. In *Proceedings of the IEEE/CVF conference on computer vision and pattern recognition*, pages 14933–14943, 2021. 3

[42] Anh Nguyen, Alexey Dosovitskiy, Jason Yosinski, Thomas Brox, and Jeff Clune. Synthesizing the preferred inputs for neurons in neural networks via deep generator networks. *Advances in neural information processing systems*, 29, 2016. 3

[43] Chris Olah, Alexander Mordvintsev, and Ludwig Schubert. Feature visualization. *Distill*, 2017. doi: 10.23915/distill.00007. <https://distill.pub/2017/feature-visualization>. 3

[44] Bruno A Olshausen and David J Field. Emergence of simple-cell receptive field properties by learning a sparse code for natural images. *Nature*, 381(6583): 607–609, 1996. 3

[45] Kenny Peng, Rajiv Movva, Jon Kleinberg, Emma Pearson, and Nikhil Garg. Use sparse autoencoders to discover unknown concepts, not to act on known concepts. *arXiv preprint arXiv:2506.23845*, 2025. 2, 3

[46] Joana Pereira, Adam J Simpkin, Marcus D Hartmann, Daniel J Rigden, Ronan M Keegan, and Andrei N Lupas. High-accuracy protein structure prediction in casp14. *Proteins: Structure, Function, and Bioinformatics*, 89(12):1687–1699, 2021. 1

[47] Ilan Price, Alvaro Sanchez-Gonzalez, Ferran Alet, Tom R Andersson, Andrew El-Kadi, Dominic Masters, Timo Ewalds, Jacklynn Stott, Shakir Mohamed, Peter Battaglia, et al. Probabilistic weather forecasting with machine learning. *Nature*, 637(8044):84–90, 2025. 1, 3

[48] Colorado J Reed, Ritwik Gupta, Shufan Li, Sarah Brockman, Christopher Funk, Brian Clipp, Kurt Keutzer, Salvatore Candido, Matt Uyttendaele, and Trevor Darrell. Scale-mae: A scale-aware masked autoencoder for multiscale geospatial representation learning. In *Proceedings of the IEEE/CVF International Conference on Computer Vision*, pages 4088–4099, 2023. 1

[49] Yusuf H Roohani, Tony J Hua, Po-Yuan Tung, Lexi R Bounds, Feiqiao B Yu, Alexander Dobin, Noam Teyssier, Abhinav Adduri, Alden Woodrow, Brian S Plosky, et al. Virtual cell challenge: Toward a turing test for the virtual cell. *Cell*, 188(13):3370–3374, 2025. 1

[50] Ramprasaath R Selvaraju, Michael Cogswell, Abhishek Das, Ramakrishna Vedantam, Devi Parikh, and Dhruv Batra. Grad-cam: Visual explanations from deep networks via gradient-based localization. In *Proceedings of the IEEE International Conference on Computer Vision*, 2017. 1, 3

[51] Oriane Siméoni, Gilles Puy, Huy V Vo, Simon Roburin, Spyros Gidaris, Andrei Bursuc, Patrick Pérez, Renaud Marlet, and Jean Ponce. Localizing objects with self-supervised transformers and no labels. *arXiv preprint arXiv:2109.14279*, 2021. 3

[52] Oriane Siméoni, Huy V Vo, Maximilian Seitzer, Federico Baldassarre, Maxime Oquab, Cijo Jose, Vasil Khalidov, Marc Szafraniec, Seungeun Yi, Michaël Ramamonjisoa, et al. Dinov3. *arXiv preprint arXiv:2508.10104*, 2025. 2, 4, 7, 8

[53] Karen Simonyan, Andrea Vedaldi, and Andrew Zisserman. Deep inside convolutional networks: Visualising image classification models and saliency maps. *arXiv preprint arXiv:1312.6034*, 2013. 1, 3

[54] Samuel Stevens, Jiaman Wu, Matthew J Thompson, Elizabeth G Campolongo, Chan Hee Song, David Edward Carlyn, Li Dong, Wasila M Dahdul, Charles Stewart, Tanya Berger-Wolf, Wei-Lun Chao, and Yu Su. Bio-CLIP: A vision foundation model for the tree of life. In *Proceedings of the IEEE/CVF Conference on Computer Vision and Pattern Recognition (CVPR)*, pages 19412–19424, 2024. 3

[55] Mukund Sundararajan, Ankur Taly, and Qiqi Yan. Axiomatic attribution for deep networks. In *International conference on machine learning*, pages 3319–3328. PMLR, 2017. 1, 3

[56] Adly Templeton, Tom Conerly, Jonathan Marcus, Jack Lindsey, Trenton Bricken, Brian Chen, Adam Pearce, Craig Citro, Emmanuel Ameisen, Andy Jones, Hoagy Cunningham, Nicholas L Turner, Callum McDougall, Monte MacDiarmid, C. Daniel Freeman, Theodore R. Sumers, Edward Rees, Joshua Batson, Adam Jermyn, Shan Carter, Chris Olah, and Tom Henighan. Scaling monosemanticity: Extracting interpretable features from claude 3 sonnet. *Transformer Circuits Thread*, 2024. URL <https://transformer-circuits.pub/>

- [57] Grant Van Horn, Elijah Cole, Sara Beery, Kimberly Wilber, Serge Belongie, and Oisin Mac Aodha. Benchmarking representation learning for natural world image collections. In *Proceedings of the IEEE/CVF conference on computer vision and pattern recognition*, pages 12884–12893, 2021. 1
- [58] Xudong Wang, Rohit Girdhar, Stella X Yu, and Ishan Misra. Cut and learn for unsupervised object detection and instance segmentation. In *Proceedings of the IEEE/CVF conference on computer vision and pattern recognition*, pages 3124–3134, 2023. 3
- [59] Yangtao Wang, Xi Shen, Yuan Yuan, Yuming Du, Mao-mao Li, Shell Xu Hu, James L Crowley, and Dominique Vaufreydaz. Tokencut: Segmenting objects in images and videos with self-supervised transformer and normalized cut. *IEEE transactions on pattern analysis and machine intelligence*, 45(12):15790–15801, 2023. 3
- [60] Jason Wei, Yi Tay, Rishi Bommasani, Colin Raffel, Barret Zoph, Sebastian Borgeaud, Dani Yogatama, Maarten Bosma, Denny Zhou, Donald Metzler, et al. Emergent abilities of large language models. *arXiv preprint arXiv:2206.07682*, 2022. 3
- [61] Mengqi Xue, Qihan Huang, Haofei Zhang, Lechao Cheng, Jie Song, Minghui Wu, and Mingli Song. Protopformer: Concentrating on prototypical parts in vision transformers for interpretable image recognition. *arXiv preprint arXiv:2208.10431*, 2022. 3
- [62] Jason Yosinski, Jeff Clune, Yoshua Bengio, and Hod Lipson. How transferable are features in deep neural networks? *Advances in neural information processing systems*, 27, 2014. 8
- [63] Bolei Zhou, Hang Zhao, Xavier Puig, Sanja Fidler, Adela Barriuso, and Antonio Torralba. Scene parsing through ade20k dataset. In *Proceedings of the IEEE conference on computer vision and pattern recognition*, pages 633–641, 2017. 2

Appendices

1. Sec. A: Limitations
2. Sec. B: Training details and hyperparameters
3. Sec. C: Precise metric definitions
4. Sec. D: Additional qualitative examples
5. Sec. E: Detailed ablation results.

A. Limitations

Our evaluation relies on ground-truth annotations to measure concept alignment, which limits our ability to assess discovery in truly unannotated domains. We also only use visual examples to describe features; future work might use multimodal large language models to describe features in language. While strong performance on two domains suggests the method will generalize, we leave both systematic evaluation of novel discoveries and applying SAEs to non-vision foundation models to future work.

B. Training Details

Our code contains instructions to reproduce our exact findings.

SAE Training.

- Initialize W_{enc} and W_{dec} with Kaiming initialization [24] and b_{enc} and b_{dec} with all zeros.
- Train SAEs with Adam [32] for 100M examples with a batch size of 16,384.
- Linearly warmup learning rate from 0 to the maximum over 500 steps, then use cosine decay to 0.
- Linearly warmup the sparsity coefficient λ from 0 to the maximum over all of training.
- Normalize W_{dec} to have unit norm columns at every step and remove gradients parallel to the columns to avoid interactions between Adam moments and normalization [7].
- Sweep both learning rate and sparsity coefficient λ for each setting, using the values in Tab. D1.

Baseline Training. We train k -means and PCA with randomly shuffled mini-batches with a batch size of 16,384 using 100M examples.

1D Probe Training. We optimize Eq. (7) for 1-dimensional logistic regression classifiers for each pair of $\{\text{SAE latent } i, \text{class } c\}$ with a ridge of $1e-8$ and 30 steps of Newton-style optimization. We initialize w to 0 and b to the prevalence of the class c in the entire dataset.

C. Metric Definitions

We use a variety of metrics to evaluate SAE probe quality. We include scatter plots of our different metrics (Probe R , mAP, Purity@ k and Coverage@ τ) in Fig. C1.

Hyperparam	Sweep Values
Learning Rate	$[3e-4, 1e-3, 3e-3, 1e-2, 3e-2, 1e-1]$
Sparsity Coeff.	$[1e-4, 1e-3, 1e-2, 1e-1]$

Table D1. Sparse autoencoder hyperparameter sweep values.

Probe R . We record the binary cross entropy loss (see Eq. (7)) for the trained probe (\mathcal{L}) and the loss for a bias-only probe (\mathcal{L}_π). We normalize the trained loss by the bias-only loss: $1 - (\mathcal{L}/\mathcal{L}_\pi)$.

mAP. For each class, we treat its patches as positives and all others as negatives, rank all validation patches by the corresponding probe score, and compute average precision as the area under the precision–recall curve. We report mean average precision (mAP) as the macro-average of per-class AP values, assigning AP=0 to classes without positive examples.

Purity@ k . For each SAE latent i , we take the k image patches that maximally activate latent i and measure how many of the k patches have the same patch label, then normalize by k to get a score between 0 and 1. We set $k=16$ in our work.

Coverage@ τ . We measure the fraction of classes (151 for ADE20K, 10 for FishVista) who have an SAE latent with a minimum average precision of τ . We set $\tau=0.3$ in our work.

D. Qualitative Examples

We show additional qualitative examples of both success and failure for ADE20K classes for all methods in Fig. D2.

E. Ablation Results

We report all metrics for the best SAE for each ViT size and layer in Tab. E2.

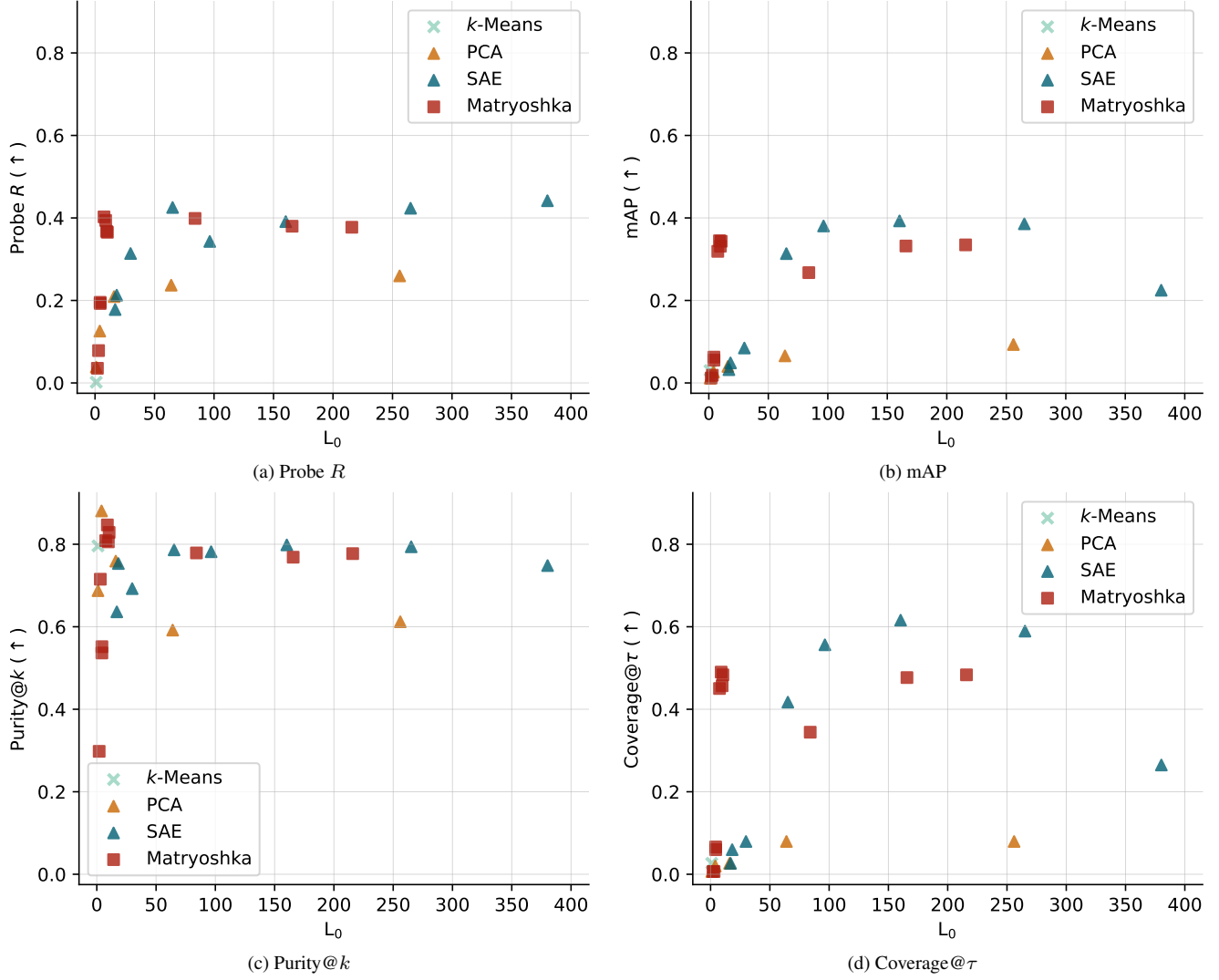


Figure C1. We compare *k*-means, PCA, vanilla SAEs and Matryoshka SAEs against sparsity (L_0) and downstream metrics (Probe R , mAP, Purity@ k and Coverage@ τ) for ADE20K.

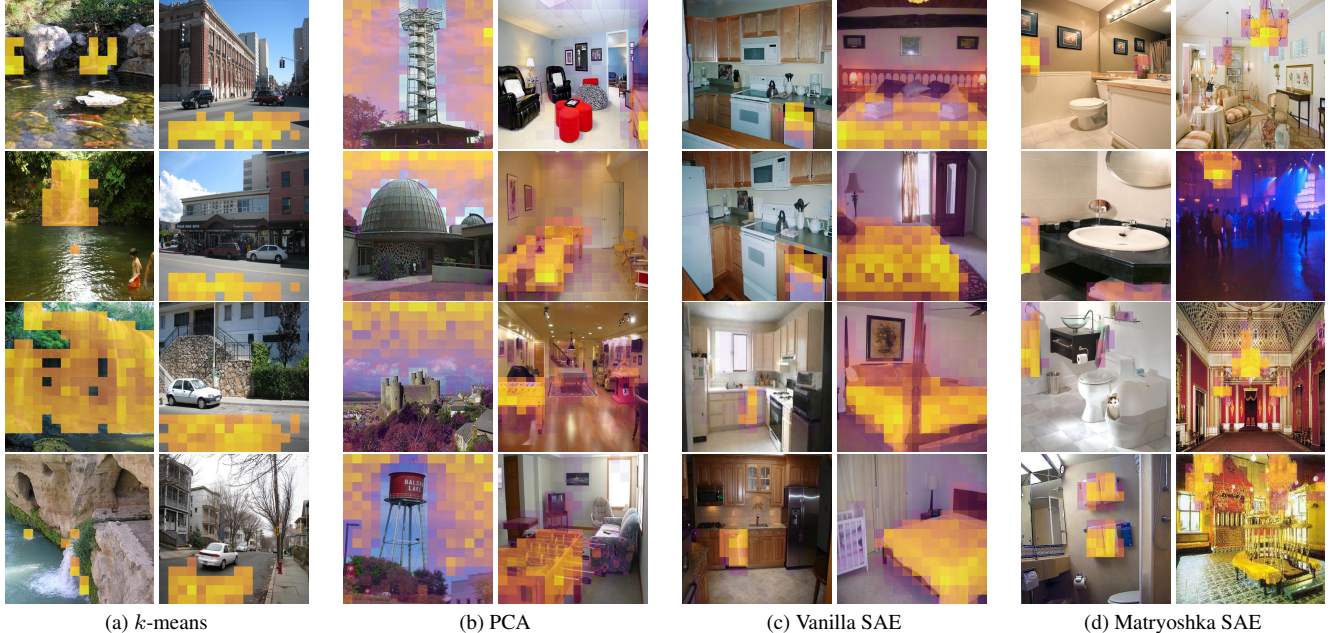


Figure D2. Some additional qualitative examples for (a) k -means: “waterfall” (left) and “road” (right), (b) PCA: “sky” (left) and “pooltable” (right), (c) vanilla SAEs: “dishwasher” (left) and “bed” (right) and (d) Matryoshka SAEs: “towel” (left) and “chandelier” (right).

Table E2. Probe results for Matryoshka SAEs trained on ImageNet-1K and evaluated on ADE20K. For each layer in each size of ViT, we choose the best SAE based on training probe loss and report all dictionary learning and downstream metrics. A summary of these results is presented in Secs. 4.3 and 4.4.

Model		Dict. \downarrow		Downstream \uparrow			
Size	Layer	NMSE	L_0	Probe R	mAP	Purity@ k	Coverage@ τ
ViT-S/16	7	0.182	70.9	0.165	0.044	0.744	0.053
ViT-S/16	8	0.143	135.1	0.209	0.062	0.623	0.086
ViT-S/16	9	0.133	159.8	0.232	0.071	0.511	0.086
ViT-S/16	10	0.299	84.1	0.251	0.099	0.626	0.093
ViT-S/16	11	0.438	23.6	0.310	0.160	0.645	0.205
ViT-S/16	12	0.294	95.1	0.434	0.203	0.742	0.245
ViT-B/16	7	0.572	19.5	0.216	0.055	0.548	0.066
ViT-B/16	8	0.497	35.4	0.240	0.061	0.516	0.073
ViT-B/16	9	0.571	10.7	0.265	0.109	0.613	0.126
ViT-B/16	10	0.431	20.1	0.322	0.191	0.607	0.272
ViT-B/16	11	0.271	47.5	0.379	0.246	0.661	0.371
ViT-B/16	12	0.359	89.9	0.441	0.312	0.812	0.430
ViT-L/16	14	0.252	90.7	0.210	0.076	0.523	0.079
ViT-L/16	16	0.336	92.4	0.266	0.117	0.575	0.152
ViT-L/16	18	0.659	11.8	0.261	0.090	0.533	0.099
ViT-L/16	20	0.471	22.2	0.263	0.152	0.582	0.179
ViT-L/16	22	0.380	35.3	0.313	0.267	0.655	0.384
ViT-L/16	24	0.703	6.5	0.403	0.319	0.809	0.450